Published in final edited form as:
Cancer Res. 2014 November 15; 74(22): 6463–6473. doi:10.1158/0008-5472.CAN-13-2922.

Histone H1.3 suppresses *H19* noncoding RNA expression and cell growth of ovarian cancer cells

Magdalena Medrzycki[1,2,*], **Yunzhe Zhang**[1,2], **Weijia Zhang**[3], **Kaixiang Cao**[1,2], **Chenyi Pan**[1,2], **Nathalie Lailler**[4], **John F. McDonald**[1,2], **Eric E. Bouhassira**[5], and **Yuhong Fan**[1,2,#]

[1]School of Biology, Georgia Institute of Technology, 310 Ferst Drive, Atlanta, GA, 30332, USA

[2]The Petit Institute for Bioengineering and Bioscience, Georgia Institute of Technology, 315 Ferst Drive, Atlanta, GA 30332, USA

[3]Department of Medicine, Icahn School of Medicine at Mount Sinai, New York, NY 10029

[4]Memorial Sloan-Kettering Cancer Center, New York, NY 10065, USA

[5]Department of Cell Biology, Albert Einstein College of Medicine, Bronx, NY 10461, USA

Abstract

Ovarian cancer is a deadly gynecological malignancy for which novel biomarkers and therapeutic targets are imperative for improving survival. Previous studies have suggested the expression pattern of linker histone variants as potential biomarkers for ovarian cancer. To investigate the role of histone H1 in ovarian cancer cells, we characterize individual H1 variants and overexpress one of the major somatic H1 variants, H1.3, in OVCAR-3 epithelial ovarian cancer cell line. We find that overexpression of H1.3 decreases the growth rate and colony formation of OVCAR-3 cells. We identify histone H1.3 as a specific repressor for the non-coding oncogene *H19*. Overexpression of H1.3 suppresses *H19* expression and knockdown of H1.3 increases its expression in multiple ovarian epithelial cancer cell lines. Furthermore, we demonstrate that histone H1.3 overexpression leads to increased occupancy of H1.3 at the *H19* regulator region encompassing the imprinting control region (ICR), concomitant with increased DNA methylation and reduced occupancy of the insulator protein CTCF at the ICR. Finally, we demonstrate that H1.3 overexpression and *H19* knockdown synergistically decreases the growth rate of ovarian cancer cells. Our findings suggest that H1.3 dramatically inhibits *H19* expression which contributes to the suppression of epithelial ovarian carcinogenesis.

Keywords

Linker histones; H1 variants; H1.3; *H19*; noncoding RNA; ovarian cancer; epigenetic marks

[#]**Corresponding author**: Yuhong Fan, PhD, School of Biology and the Petit Institute for Bioengineering and Bioscience, Georgia Institute of Technology, IBB 2313, 315 Ferst Drive, Atlanta, GA 30332-0363, USA, Yuhong.fan@biology.gatech.edu; Phone: 404-385-1312; Fax: 404-894-0519.
[*]Current address: School of Medicine, Emory University, Atlanta, GA 30322

The authors disclose no potential conflicts of interest

Introduction

Ovarian cancer has the highest mortality rate among gynecological malignancies, and is currently the fourth most common cancer in women. Each year, more than 22,000 women are diagnosed with ovarian cancer in the US and about 15,000 women die of the disease, primarily due to difficulties in early diagnosis and poor prognosis (1, 2). The etiology of ovarian cancers involves both genetic and epigenetic alterations, although the underlying mechanisms are not well understood ((3–5) and references therein). Recently, the expression of linker histone variants has been suggested as potential biomarkers for ovarian cancers (6). However, the role of linker histone variants in ovarian cancer cells has not been explored.

H1 linker histones interact with the nucleosomes at the entry and exit sites of the nucleosomal DNA and facilitate the folding of chromatin into higher order structures (7). In mammals, there are 11 H1 variants identified, including 7 somatic H1 variants (H1.0 to H1.5, and H1.x), and 4 tissue specific H1s (testis-specific H1t, H1T2, HILS1, and oocyte-specific H1oo) (8). H1.1 to H1.5, are 5 major somatic H1 variants in both dividing and non-dividing cells, whereas H1.0 mainly accumulates in differentiated cells. H1x is present in very low amount and found to have a higher expression in neuroendocrine cells (8). The heterogeneity and expression pattern of H1s are conserved from mouse to human, suggesting that the individual variants may have unique properties and functions.

Besides mediating higher order chromatin folding, linker histone H1 has been shown to regulate gene expression *in vivo* in a specific manner (9). However, it is not clear whether those genes are directly regulated by a specific H1 variant. Here, we report the identification of an important non-coding *H19* gene as a direct target specifically regulated by H1.3 in ovarian cancer cells.

Aberrant expression of *H19* occurs in ovarian cancer and other types of cancers (10–12). *H19* is often overexpressed in ovarian cancer, and has been suggested as a biomarker for ovarian cancer (13). Ample studies show that *H19* is essential for tumor growth and *H19* overexpression contributes to tumorigenesis (reviewed in (14)), although its role in ovarian cancer has not been well studied. *H19* is an oncofetal gene located on human chromosome 11 and is highly expressed in fetal tissues but suppressed in most tissues after birth (15, 16). *H19* belongs to an imprinted gene family controlled by the imprinting control region (ICR) which is important for mammalian development (17, 18). Expressed from the maternal allele, *H19* encodes for a spliced, capped and polyadenylated non-coding RNA highly conserved in evolution (19). It is also a precursor for a microRNA, miR-675, which targets genes essential for growth, development and carcinogenesis, such as RB and Igf1r (20–22). The *H19* locus was recently found to produce antisense transcripts, including *H19* opposite tumor suppressor (HOTS) and a long intergenic transcript, 91H, indicating the complexity of this region (23, 24). Moreover, *H19* expression has been shown to be regulated by chromatin structure and epigenetic mechanisms, including DNA methylation, CTCF insulator and enhancer activities (reviewed in (25, 26)).

In this study, we utilize overexpression and shRNA knockdown approaches to modulate the expression levels of H1s and *H19* mRNA in OVCAR-3 cells. We find that linker histone

H1.3 directly represses the expression of *H19* gene in ovarian epithelial cancer cells by preferential occupancy at the ICR of *H19* and regulating DNA methylation at this region. We also show that H1.3 overexpression suppresses the growth and clonogenicity in ovarian cancer cells, has synergistic effects with *H19* knockdown on inhibition of epithelial ovarian cancer cells. These results suggest H1.3 as a potent epigenetic regulator for *H19* and a novel mechanism by which H1.3 suppresses tumorigenesis in epithelial ovarian cancer cells.

Materials and Methods

Cell culture

OVCAR-3 cells were cultured in RPMI-1640 (Fisher) media supplemented with 20% fetal bovine serum (FBS) (Gemini), 100 U/ml penicillin and 100 mg/ml streptomycin (Life Technologies). OV-90 cells were cultured in a 1:1 mixture of MCDB 105 medium (Sigma) and medium 199 (Sigma) supplemented with 15% FBS, 1.85 g/L sodium bicarbonate and 100 U/ml penicillin and 100 mg/ml streptomycin. SK-OV-3 cells were cultured in McCoy's 5a Medium modified medium (Sigma) supplemented with 10% FBS, 2.2 g/L sodium bicarbonate and 100 U/ml penicillin and 100 mg/ml streptomycin. All cells were cultured in a humidified incubator with 5% CO_2 at 37°C.

Vectors construction, cell transfection and stable cell lines generation

The coding sequences of human H1 variant genes were cloned into a modified pcDNA3 vector with FLAG sequence (5'-GACTACAAAGACGATGACGACAAG-3') at the N-terminal to the start codon and sequence verified. The vector containing *H19* gene was purchased from Genescript and the *H19* gene was inserted into pcDNA3 vector and sequence verified.

OVCAR-3 cells were transfected with pcDNA-H1s or pcDNA-*H19* vectors by Lipofectamine 2000 (Life Technologies) according to the manufacturer's manual. Two days post-transfection, the cells were treated with 400 μg/ml G418 (Geneticin, Life Technologies) for 4 to 5 weeks and resistant clones were isolated and screened. OV-90 cells were transfected with H1.1 or H1.3 expression vectors by Nucleofector™ Kits (Lonza) following the manufacturer's protocol and cells were harvested two days post transfection and analyzed.

pTRIPz (inducible), pGIPz (stable) shRNA vectors and TransLenti Viral Packaging systems were purchased from Thermo Scientific. Viral particles containing vectors expressing shRNA for *H19* or H1.3 were produced according to the manufacturer's manual, and used to transduce OVCAR-3, OV-3/H1.3(H), SK-OV-3 cells. The cells were subsequently sorted (BD FACS Aria III Cell Sorter, Beckman Coulter) by Red Fluorescence Protein (RFP) or Green Fluorescence Protein (GFP) expression to enrich the shRNA expressing cells.

RNA isolation and RT-PCR

RNAs were extracted with Trizol (Life Technologies) according to the manufacturer's instructions and further cleaned using RNeasy Mini kit (Qiagen). 2.5 μg of total RNA were reverse transcribed using Superscript III kit (Life Technologies) according to the

manufacturer's protocol and cDNAs were subsequently analyzed by quantitative real-time PCR (qRT-PCR). *H19* primers were as follows: F: 5'-ACCACTGCACTACCTGACTC-3' and R: 5'-CCGCAGGGGGTGGCCATGAA-3'. *GAPDH* primers were published previously (6). The relative expression of selected genes were quantified and analyzed by real-time PCR using iQ SYBR Green PCR Supermix kit (Bio-Rad Laboratories) as previously described (27). All samples were typically analyzed in triplicates in at least 3 independent runs.

Western blotting

The cells were lysed in Lysis buffer (30 mM Tris pH 8.0, 150 mM NaCl, 0.1% SDS, 0.5% Na-deoxycholate, 0.1% NP-40, Proteinase Inhibitor tablet (Roche)) and total histones were extracted as previously described (27). Western blotting assays were performed according to the manufacturer's manual (Bio-Rad). The primary antibodies used are against: FLAG-tag (Sigma, F1804), H1.2 (Abcam, ab4086), H1.3 (Abcam, ab24174), phospho-H1.4 (Sigma, H7664), H1.5 (Abcam, ab24175), H1.0 (Santa Cruz, sc-56695), beta-actin (Sigma, A5441). The secondary antibodies are: IRDye680 Goat anti-Rabbit (Li-COR, 926–32221), IRDye800 Goat anti-Rabbit (Rockland, 611-0132-122) or Goat anti-Mouse (Molecular Probes, A21058). Signals were visualized using Odyssey Infrared Imaging System (LI-COR Biosciences).

Growth curves, MTT and clonogenic assays

For growth curves and MTT cell proliferation assays, 3×10^4 cells per well in 12 well plate and 1500 cells per well in 96-well plate were seeded in triplicates, respectively. Cell numbers were counted with Multisizer Coulter Counter (Beckman Coulter) and MTT assay were performed every two days for indicated days. Values are expressed as mean ± SD and statistical analyses were performed using GraphPad Prism statistical software. For MTT assay, two hours after incubation with MTT compound (Sigma), mitochondrial succinate dehydrogenase in metabolically active cells formed insoluble formazan crystals, which were resolubilized with stop solution (10% SDS, 0.1% HCl). The amount of formazan crystals produced by the cells was proportional to metabolic activity, which was measured by spectrometer at 570 nm wavelength. For colony forming assay, 100, 300, and 1000 cells were seeded on 3.5-cm dishes in triplicates and were cultured in a humidified incubator with 5% CO_2 for 4 weeks as previously described with modifications (28). Medium was changed every 3 days. After incubation, the cell colonies were fixed with PBS:Methanol (1:1 ratio) for 2 minutes, then incubated in Methanol for 10 minutes, and air dried. The colonies were stained by adding 3 ml 1% Crystal violet for 10 minutes and counted.

Microarray and data analysis

Total RNAs were isolated with TRIzol reagent (Life Technologies), purified, labeled and used for microarray hybridization to human Affymetrix ST1.0 array at Einstein Genomic Facility. Data were analyzed using RMA normalization in Expression Console (Affymetrix). Selected gene changes were confirmed using qRT-PCR. The results were normalized over the housekeeping gene *GAPDH* and compared with the controls. Cluster analysis was performed to group genes with altered expression more than 2-fold into subgroups according

to their expression patterns (Cluster 3.0). Differentially expressed genes were analyzed with Ingenuity Pathway Analysis (IPA) Software (Qiagen) to determine the pathways or functional groups of genes involved. Gene ontology analysis was performed using DAVID (29) to obtain enriched biological processes categories of statistical significance. Microarray data are available at the NCBI Gene Expression Omnibus (GEO) database under accession number GSE61692.

High Performance Liquid Chromatography

Histone proteins were extracted using 0.2 N sulfuric acid as previously described (27). 100 μg of total histone preparations were injected into a C18 reverse phase column (Vydac) on an AKTA UPC10 system (GE Healthcare). Fractions corresponding to the H1.2/H1.3/H1.4 peak from HPLC analysis were collected and subjected to mass spectrometry analysis on a Qstar XL MS/MS system (Applied Biosystems) with electrospray ionization (ESI) as the ionization method. Analyst QS software (Applied Biosystems) was used for data acquirement and analysis.

Chromatin Immunoprecipitation, qChIP and ChIP-seq

ChIP assays were performed as previously described (30) with modifications. The following antibodies were used: anti-FLAG (Sigma, F1804), anti-CTCF (Santa Cruz, Sc15914), and anti-IgG (Millipore, 12–370). Purified ChIP-DNA quantified using Qubit Fluorometer (Life Technologies). For qChIP, the amount of each specific DNA fragment in immuno-precipitates was determined by real-time PCR. PCR reactions were prepared with the iQ SYBR Green Supermix (Bio-Rad) and were analyzed in a MyIQ Real-Time PCR Detection System (Bio-Rad). All samples were typically analyzed in triplicates in three independent experiments. For ChIP-seq, the libraries for massive parallel sequencing were prepared with the ChIP-seq Sample Preparation Kit (Illumina) according to the manufacturer's instructions. Sequencing was performed with Illumina HiSeq 2000 systems. Sequence reads processing, alignment and metagene analysis were performed as previously described (31).

Bisulfite sequencing analysis

Genomic DNA was isolated from cells with QIAamp DNA kit (Qiagen). 1 μg of DNA was treated with the CpGenome™ DNA Modification kit (Millipore) according to the manufacturer's manual. Treated DNA was dissolved in 25 μl H_2O, and 1 μl of treated DNA was used in each PCR reaction as previously described (9). The following primers were used: *H19* region 1: forward, 5'-TTGTAAGTGTGGATTTAAAAGT-3', reverse, 5'-ACAATTATCAATTCAAA AAAAA-3'; *H19* region 2: 5'-TTTTGGAGGTTTTTTTTTA-3', 5'-AAACCCTACAA CACCTAACT-3'; *H19* region 3: 5'-GGTGGTAGGAAGGGGTTTTT-3', 5'-CCCAACACCCA TCCTAAAAT-3'. The PCR products were subsequently cloned using the TOPO TA cloning kit (Life Technologies), and clones containing the converted DNA inserts were selected for sequencing. DNA sequences were analyzed with BiQ analyzer.

Results

Analysis of individual H1 variants in OVCAR-3 cells

OVCAR-3 cell line is a well-characterized epithelial ovarian cancer cell line frequently used to study molecular mechanisms of ovarian cancer malignancies. This cell line was derived from a patient with epithelial ovarian adenocarcinomas, which represent about 90% of all ovarian cancer malignancies. We first characterized the expression of individual histone H1 variants by HPLC, Mass Spectrometry and Western blotting assays. Total histones were isolated from OVCAR-3 cells by sulfuric acid extraction and subjected to RP-HPLC (Fig. 1A). Three fractions of putative H1 variants were collected, lyophilized and analyzed by Mass spectrometry and Western blotting. The fraction 3 was identified as a mixture of histones H1.2, H1.3 and H1.4 (Fig. 1A and B), three major somatic H1 variants abundantly expressed in adult tissues and cells. However, we noted that H1.3 protein level is much lower than H1.2 and H1.4 in OVCAR-3 cells, which is unusual given that histone H1.3 is ubiquitously expressed among different cell types and that H1.3 mRNA transcripts were present at high levels in OVCAR-3 (data not shown). To verify the identity of individual peaks of the HPLC fractions, we generated 6 stable cell lines with each overexpressing one of the six somatic histone H1 variants (H1.0-H1.5) in OVCAR-3 cells (designated as OV-3/H1 lines) (Fig. 1C). All 6 overexpressed somatic H1 variants were tagged by FLAG at the N-terminus, which was expected to maintain biochemical properties and functions of the respective H1 variants (31). The total histones were extracted and analyzed by HPLC and the eluted fractions were collected and verified by Western blotting (Fig. 1C). These results demonstrate the peak identity and the relative amount of each linker histone variant in HPLC profile from OVCAR-3/H1 cell lines.

Overexpression of histone H1.3 inhibits cell growth and colony formation

Histone H1.3 is one of the major somatic H1 variants abundantly present in both dividing and non-dividing cells. The very low expression of endogenous H1.3 in OVCAR-3 cells provides a good experimental system for us to investigate the role of H1.3 in ovarian cancer cells using an overexpression approach. We generated multiple OV-3/H1.3 stable clones by overexpressing FLAG-H1.3 in OVCAR-3 cells and screened 48 clones by Western blotting using an anti-FLAG antibody (Supplementary Fig. S1A). HPLC/MS analysis of the histone extracts from the clone with the highest FLAG-H1.3 level (designated as OV-3/H1.3(H)) as well as Western blotting assays using anti-H1 variant antibodies demonstrated that FLAG-H1.3 co-eluted in the same fraction as the endogenous H1.3, suggesting similar biochemical properties of FLAG-H1.3 as the endogenous H1.3 (Fig. 1A, B, and D). Western blotting and calculation of the individual H1 to nucleosome ratio from HPLC analysis indicated that the protein level of FLAG-H1.3 in OVCAR-3/H1.3(H) cells was significant, reaching ∼16% of the total H1s in these cells (Fig. 1D and E).

To characterize the phenotypic changes caused by H1.3 overexpression, we compared the growth rate, metabolic activity, and colony forming abilities of OVCAR-3 and OV-3/H1.3(H). OV-3/H1.3(H) cells displayed reduced growth rate by growth curve and MTT assays (Fig. 2A). Knocking down H1.3 in OV-3/H1.3(H) cells by shRNA (Supplementary Fig.S1B) reverted this effect (Fig. 2A). These results indicated that overexpression of H1.3

variant reduces cell proliferation and affects the metabolic activity in OVCAR-3. In addition, the clonogenic capacity of OV-3/H1.3(H) cells was severely impaired, forming 10 to 15 times fewer colonies than OVCAR-3 cells (Fig. 2B). This inhibitory effect of overexpression of H1.3 on colony formation was partially abolished by H1.3 knockdown using shRNA in OV-3/H1.3(H) cells (Fig. 2B).

Overexpression of H1.3 leads to specific changes in gene expression

To identify genes and pathways affected by H1.3 overexpression, we performed gene expression profiling using Affymetrix Human Gene 1.0 ST Arrays. Comparison of the transcriptomes of OV-3/H1.3(H) cells with control cell lines of OVCAR-3 transfected with vectors without H1.3 (designated as OV-3/V.O.) showed that 164 genes had altered gene expression more than 2 fold in both replicated experiments. Among these genes, 76 were upregulated and 88 were downregulated in OV-3/H1.3(H) cells (Fig. 2C and Supplementary Table S1). Results from RT-PCR of several differentially expressed genes showed expression changes comparable to that from microarrays (Supplementary Fig. S2). Analysis of the molecular pathways and cellular processes altered in OV-3/H1.3(H) cells using Ingenuity Pathway Analysis (IPA) software indicated that cell proliferation, cell adhesion, programmed cell death, cell migration and immune response were all affected. A representative IPA hit map of cell function and maintenance including *H19* gene is shown in Figure 2D. Gene ontology classification using DAVID (29) revealed that upregulated genes are mainly enriched in immune response and antigen presentation whereas downregulated genes are involved in a variety of biological processes, such as regulation of cell proliferation, cell communication, signal transduction and various metabolic processes (Fig. 2E and Supplementary Table S2).

Oncogene *H19* is a direct target of H1.3

One of the most dramatically dysregulated genes in OVCAR-3 cells is *H19*, which was repressed 9-fold in OV-3/H1.3(H) cells, ranked #2 in the most highly repressed genes (Supplementary Table S1). Expressing FLAG-H1.3 to low-medium level in OV-3/H1.3(L) cells (Supplementary Fig. S1A) resulted in a medium reduction in *H19* expression (Fig. 3A), indicating a dosage-dependent effect of H1.3 on *H19* expression. Knockdown histone H1.3 levels by stably expressing shRNA against H1.3 in OV-3/H1.3(H)/shH1.3 cells (Supplementary Fig. S1B) alleviated the repression of *H19* by H1.3, whereas scrambled shRNA did not have any effects (Fig. 3A). To further test if the expression of *H19* is directly dependent on the amount of histone H1.3, we generated OV-3/shH1.3(i) cell line in which the expression of endogenous H1.3 in OVCAR-3 cells was knocked down more than 60% upon induction of the expression of H1.3 shRNA by Doxycycline (Fig. 3B). This knockdown led to a 50% elevation in *H19* mRNA transcripts (Fig. 3B). To investigate if *H19* expression is affected specifically by H1.3 or by all H1 variants, we analyzed *H19* expression in all 6 OV-3/H1 cell lines which exhibited comparable levels of exogenous FLAG-H1s for each respective H1 variant (Fig. 3C). *H19* transcript level was dramatically suppressed in OV-3/H1.3 line as measured by RT-PCR, but remained unchanged in cell lines overexpressing other FLAG-H1 variants in OVCAR-3 cells (Fig. 3C). These results indicate that *H19* is strongly and specifically repressed by H1.3 variant in OVCAR-3 cells.

Overexpression of H1.3 in OV-90, another ovarian epithelial cancer cell line with low expression of H1.3, also dramatically inhibited *H19* expression and cell growth, whereas these effects were not observed when H1.1 was overexpressed in OV-90/H1.1 cells (Supplementary Fig. S3A). In contrast, knockdown of H1.3 by shRNA in SK-OV-3, an ovarian epithelial cell line with higher H1.3 protein levels, resulted in a two-fold increase of *H19* expression as well as a modest increase in cell growth rate (Supplementary Fig S3B). Collectively, these results further support a specific inhibitory role of H1.3 on *H19* expression and cell growth in ovarian epithelial cancer cells.

Epigenetic mechanisms of *H19* repression mediated by H1.3

Chromatin structure and epigenetic mechanisms play a key role in *H19* expression regulation (32). To investigate the potential mechanisms by which H1.3 regulates *H19* expression in OVCAR-3 cells, we first analyzed the binding profiles of H1.3 across the entire *H19* gene locus, including a 5.2 kb upstream regulatory region, by chromatin immunoprecipitation (ChIP). H1.3 overexpression resulted in preferential accumulation of H1.3 at the entire *H19* regulatory region, but H1.3 remained absent at the house keeping gene *GAPDH* (Fig. 4). While H1.1 exhibited similarly low endogenous expression as H1.3 in OVCAR-3 cells (Fig. 1E), overexpression of FLAG-H1.1 in OVCAR-3 cells to comparable levels of FLAG-H1.3 in OV-3/H1.3(H) cells did not lead to such enriched occupancy at *H19* locus (Supplementary Fig. S4A). Genome-wide analysis of H1.3 occupancy in OV-3/H1.3(H) cells by ChIP-seq confirmed the depletion of H1.3 at active promoters and the overrepresentation of H1.3 at *H19* upstream regulatory region compared with neighboring regions (Supplementary Fig. S5).

H19 expression is controlled by the imprinting control region (ICR) located within the *H19* upstream regulatory region. In humans, this region contains 7 CTCF binding sites, of which methylation status regulates binding of the insulator binding protein CTCF (33, 34) and *H19* expression. To determine if increased H1.3 binding at *H19* ICR leads to changes in DNA methylation at *H19* ICR and CTCF binding status, we analyzed the levels of DNA methylation and CTCF occupancy at this region by bisulfite sequencing and ChIP, respectively. Such analysis indicated that *H19*-ICR region is hypomethylated in OVCAR-3 (Fig. 5A). While the global DNA methylation levels were not changed by H1.3 overexpression, as indicated by unchanged sensitivity to methylation-sensitive enzymes (Fig. 5B), DNA methylation levels of CpG sites surrounding CTCF binding sites were significantly increased in OV-3/H1.3(H) cells by 2.3- and 5.8-fold for region 1 and region 2 respectively (Fig. 5). This level of increase in DNA methylation in OV-3/H1.3(H) cells was diminished by knockdown of H1.3 by shRNA (Fig. 5), indicating that the increased occupancy of H1.3 at *H19* distal promoter region leads to hypermethylation of the *H19*-ICR. In addition, compared with OVCAR-3 cells, CTCF occupancy at *H19*-ICR was reduced at region 1 and region 2 in OV-3/H1.3(H) cells, but not in OV-3/H1.1(H) cells (Fig. 6 and Supplementary Fig. S4B). The reduced occupancy of CTCF protein on *H19*-ICR in OV-3/H1.3(H) cells suggests that overexpression of histone H1.3 may prevent CTCF from binding to the *H19* ICR region and regulating *H19* expression in OVCAR-3 cells.

Taken together, these findings suggest that linker histone H1.3 directly regulates *H19* expression in ovarian cancer cells by binding to *H19*-ICR, increasing DNA methylation and preventing CTCF from binding to CTCF sites in *H19* ICR.

Overexpression of histone H1.3 and reduction of *H19* synergistically suppress ovarian cancer cell growth

Expression of *H19* mRNA promotes proliferation and enhances tumorigenesis in several types of cancer cells (35–38). To determine if the inhibitory effect of H1.3 on OVCAR-3 growth rate is mediated through its repression on *H19* expression, we first investigated the effects of modulation of *H19* expression on OVCAR-3 growth. Overexpressing *H19* in OVCAR-3 by transfecting the cells with a pcDNA-*H19* vector dramatically increased *H19* transcripts (Fig. 7A). This upregulation resulted in significant increase in cell growth rate in OVCAR-3 (Fig. 7B). We were only able to moderately overexpress *H19* in OVCAR-3/H1.3(H) cells, which led to a moderate increase in growth rate of OVCAR-3/H1.3(H) cells, indicating that the growth inhibition in OVCAR-3 by H1.3 overexpression can be partially rescued by *H19* upregulation.

We next determined whether overexpression of H1.3 and depletion of *H19* transcript would synergistically impair the growth of ovarian cancer cells by further knocking down *H19* transcript in OV-3/H1.3(H) cells using *H19* shRNA. Induction of *H19* shRNA led to a 75% and a 92% reduction of *H19* expression in OVCAR-3 and OV3/H1.3(H) cells, respectively (Fig. 7C). Depletion of *H19* significantly reduced growth rate (Fig. 7D), suggesting that overexpression of linker histone H1.3 and depletion of *H19* transcript synergistically suppress the growth of OVCAR-3 cells.

Discussion

H19 is an oncofetal gene whose expression is frequently elevated in many solid tumors (10, 11, 13, 39). Its upregulation has been associated with increased proliferation, tumorigenesis, cell cycle progression and cell migration (35, 36, 40, 41). In this study, we uncovered a novel function of H1.3 in inhibiting ovarian cancer cell growth, likely mediated through repression of *H19* gene (Supplementary Fig. S6). By utilizing overexpression and knockdown approaches, we generated cell lines with modulated expression of histone H1 variants and *H19* transcript. Systematic analysis of generated clones demonstrates that linker histone H1.3 is the specific somatic H1 variant capable of effective suppression of *H19* in ovarian epithelial cancer cells. Our results also suggest that this regulation is likely to be a direct effect. In addition, overexpression of histone H1.3 represses the growth rate and colony formation ability in OVCAR-3 cells, suggesting its tumor suppressor properties. In contrast, similarly overexpressing H1.1 cells did not change the growth rate and clonogenicity of OVCAR-3 (Supplementary Fig. S4). The synergistic effect of H1.3 overexpression and *H19* depletion in ovarian cancer cells suggests a potential strategy of combining H1.3 modulation with *H19* for therapeutic intervention.

We have investigated the mechanism by which *H19* is suppressed by H1.3 and found that H1.3 preferentially accumulates at *H19* ICR, leading to increased DNA methylation and reduced binding of CTCF insulator binding protein at *H19*-ICR. These results suggest that

H1.3 epigenetically represses *H19* expression through DNA methylation as well as an antagonism between H1 and CTCF. Although a link between H1 and DNA methylation at regulating specific genes has been revealed in several previous studies (9, 42, 43), our study is the first one demonstrating a highly specific regulation of *H19* expression by a single H1 variant, H1.3 *in vivo* in ovarian cancer cells. Other H1 variants, when expressed to similar levels does not repress the expression of *H19* in OVCAR-3 cells (Fig. 3C). Likewise, stably overexpressing H1.3, but not H1.1, leads to dramatic reduction in *H19* expression and cell growth in OV-90 ovarian epithelial cancer cell line, and expressing H1.3 shRNA, but not scrambled shRNA, in SK-OV-3 ovarian epithelial cancer cells, increases *H19* expression and cell growth (Supplementary Fig. S3). The mechanism by which *H19* is specifically repressed by H1.3 through DNA methylation cannot be fully accounted by the interaction between H1 variants and DNA methyltransferases (DNMTs) ((44), and Cao, Ho, and Fan, unpublished observation), because multiple H1 variants are found to interact with DNMTs. Chromatin immunoprecipitation analysis demonstrates a preferential binding by H1.3 at *H19* locus and a reduced binding of CTCF at CTCF binding sites in OV-3/H1.3(H) cells (Fig. 4 and Fig.6). These binding patterns appear to be elicited specifically by overexpression of H1.3, as overexpression of H1.1 to similar levels does not lead to marked changes at this locus in OV-3/H1.1(H) cells (Supplementary Fig. S4A and B), suggesting a critical role of preferential binding of H1.3 at this locus in the *H19* inhibition. H1 variants have distinct biochemical properties and differ significantly in their residence time on chromatin and ability to promote chromatin condensation *in vitro*, which is likely to contribute to their specificity *in vivo* (45, 46). Other mechanisms may also contribute to the regulation of *H19* by H1.3. For example, linker histone H1 has been shown to interact with SirT1, promoting gene silencing (47). *In vitro* studies have shown that H1 interacts with heterochromatin protein HP1α (48) and stimulates polycomb repressive complex 2 (PRC2) activity (49). Therefore, the direct effect of H1.3 on *H19* gene silencing may be due to interactions between linker histone H1 and other chromatin proteins or factors. Additionally, histone H1 was found to inhibit human SWI/SNF nucleosome remodeling activity, (50), thus it is also conceivable that histone H1.3 acts as a specific repressor of *H19* gene by blocking the chromatin-remodeling complex to access the *H19* regulatory region.

Histone H1 is increasingly being suggested to contribute to epigenetic regulation in cancer cells. Understanding the underlying molecular mechanisms may lead to new approaches to manipulate gene expression. In this study we generated stable cell lines with tagged H1 variants and we established inducible system in which protein levels of histone H1 variants can be readily modulated. Those cell lines will serve as valuable tools to study the role of H1 in epigenetic regulation in cancer cells. The identification of H1.3 being a potent repressor for *H19* also suggests a novel function of H1.3 as a tumor suppressor in ovarian epithelial cancer cells.

Supplementary Material

Refer to Web version on PubMed Central for supplementary material.

Acknowledgments

This work is supported by NIH grant GM085261 (to YF) and Georgia Cancer Coalition Distinguished Cancer Clinicians and Scientists Award (to YF), and Georgia Tech. We thank Nikita Wright and Leonid Aksenov for technical support and colleagues for helpful discussions. We thank Georgia Tech Mass Spectrometry facility, Albert Einstein Epigenomics Shared Facility and Genomics Core Facility.

Financial support: NIH grant GM085261 (to Y.F.), Georgia Cancer Coalition Distinguished Scholar award (to Y.F.), and Georgia Institute of Technology.

References

1. Jemal A, Siegel R, Ward E, Hao Y, Xu J, Thun MJ. Cancer statistics, 2009. CA: a cancer journal for clinicians. 2009; 59:225–249. [PubMed: 19474385]
2. Goff BA, Mandel L, Muntz HG, Melancon CH. Ovarian carcinoma diagnosis. Cancer. 2000; 89:2068–2075. [PubMed: 11066047]
3. Schuijer M, Berns EM. TP53 and ovarian cancer. Human mutation. 2003; 21:285–291. [PubMed: 12619114]
4. Balch C, Fang F, Matei DE, Huang TH, Nephew KP. Minireview: epigenetic changes in ovarian cancer. Endocrinology. 2009; 150:4003–4011. [PubMed: 19574400]
5. Nephew KP, Balch C, Zhang S, Huang TH. Epigenetics and ovarian cancer. Cancer treatment and research. 2009; 149:131–146. [PubMed: 19763434]
6. Medrzycki M, Zhang Y, McDonald JF, Fan Y. Profiling of linker histone variants in ovarian cancer. Frontiers in bioscience : a journal and virtual library. 2012; 17:396–406.
7. Woodcock CL, Skoultchi AI, Fan Y. Role of linker histone in chromatin structure and function: H1 stoichiometry and nucleosome repeat length. Chromosome research : an international journal on the molecular, supramolecular and evolutionary aspects of chromosome biology. 2006; 14:17–25.
8. Happel N, Doenecke D. Histone H1 and its isoforms: contribution to chromatin structure and function. Gene. 2009; 431:1–12. [PubMed: 19059319]
9. Fan Y, Nikitina T, Zhao J, Fleury TJ, Bhattacharyya R, Bouhassira EE, et al. Histone H1 depletion in mammals alters global chromatin structure but causes specific changes in gene regulation. Cell. 2005; 123:1199–1212. [PubMed: 16377562]
10. Adriaenssens E, Dumont L, Lottin S, Bolle D, Lepretre A, Delobelle A, et al. *H19* overexpression in breast adenocarcinoma stromal cells is associated with tumor values and steroid receptor status but independent of p53 and Ki-67 expression. The American journal of pathology. 1998; 153:1597–1607. [PubMed: 9811352]
11. Ariel I, Miao HQ, Ji XR, Schneider T, Roll D, de Groot N, et al. Imprinted *H19* oncofetal RNA is a candidate tumour marker for hepatocellular carcinoma. Molecular pathology : MP. 1998; 51:21–25. [PubMed: 9624415]
12. Cui H, Onyango P, Brandenburg S, Wu Y, Hsieh CL, Feinberg AP. Loss of imprinting in colorectal cancer linked to hypomethylation of *H19* and IGF2. Cancer research. 2002; 62:6442–6446. [PubMed: 12438232]
13. Tanos V, Prus D, Ayesh S, Weinstein D, Tykocinski ML, De-Groot N, et al. Expression of the imprinted *H19* oncofetal RNA in epithelial ovarian cancer. European journal of obstetrics, gynecology, and reproductive biology. 1999; 85:7–11.
14. Matouk I, Raveh E, Ohana P, Lail RA, Gershtain E, Gilon M, et al. The increasing complexity of the oncofetal *H19* gene locus: functional dissection and therapeutic intervention. International journal of molecular sciences. 2013; 14:4298–4316. [PubMed: 23429271]
15. Gabory A, Ripoche MA, Yoshimizu T, Dandolo L. The *H19* gene: regulation and function of a non-coding RNA. Cytogenetic and genome research. 2006; 113:188–193. [PubMed: 16575179]
16. Ariel I, Ayesh S, Perlman EJ, Pizov G, Tanos V, Schneider T, et al. The product of the imprinted *H19* gene is an oncofetal RNA. Molecular pathology : MP. 1997; 50:34–44. [PubMed: 9208812]
17. Gabory A, Ripoche MA, Le Digarcher A, Watrin F, Ziyyat A, Forne T, et al. *H19* acts as a trans regulator of the imprinted gene network controlling growth in mice. Development. 2009; 136:3413–3421. [PubMed: 19762426]

18. Borensztein M, Monnier P, Court F, Louault Y, Ripoche MA, Tiret L, et al. Myod and *H19*-Igf2 locus interactions are required for diaphragm formation in the mouse. Development. 2013; 140:1231–1239. [PubMed: 23406902]
19. Ayesh S, Matouk I, Schneider T, Ohana P, Laster M, Al-Sharef W, et al. Possible physiological role of *H19* RNA. Molecular carcinogenesis. 2002; 35:63–74. [PubMed: 12325036]
20. Keniry A, Oxley D, Monnier P, Kyba M, Dandolo L, Smits G, et al. The *H19* lincRNA is a developmental reservoir of miR-675 that suppresses growth and Igf1r. Nature cell biology. 2012; 14:659–665.
21. Tsang WP, Ng EK, Ng SS, Jin H, Yu J, Sung JJ, et al. Oncofetal *H19*-derived miR-675 regulates tumor suppressor RB in human colorectal cancer. Carcinogenesis. 2010; 31:350–358. [PubMed: 19926638]
22. Cai X, Cullen BR. The imprinted *H19* noncoding RNA is a primary microRNA precursor. Rna. 2007; 13:313–316. [PubMed: 17237358]
23. Berteaux N, Aptel N, Cathala G, Genton C, Coll J, Daccache A, et al. A novel *H19* antisense RNA overexpressed in breast cancer contributes to paternal IGF2 expression. Molecular and cellular biology. 2008; 28:6731–6745. [PubMed: 18794369]
24. Onyango P, Feinberg AP. A nucleolar protein, *H19* opposite tumor suppressor (HOTS), is a tumor growth inhibitor encoded by a human imprinted *H19* antisense transcript. Proceedings of the National Academy of Sciences of the United States of America. 2011; 108:16759–16764. [PubMed: 21940503]
25. Sasaki H, Ishihara K, Kato R. Mechanisms of Igf2/*H19* imprinting: DNA methylation, chromatin and long-distance gene regulation. Journal of biochemistry. 2000; 127:711–715. [PubMed: 10788777]
26. Gabory A, Jammes H, Dandolo L. The *H19* locus: role of an imprinted non-coding RNA in growth and development. BioEssays : news and reviews in molecular, cellular and developmental biology. 2010; 32:473–480.
27. Medrzycki M, Zhang Y, Cao K, Fan Y. Expression analysis of mammalian linker-histone subtypes. Journal of visualized experiments : JoVE. 2012; 61:e3577.
28. Franken NA, Rodermond HM, Stap J, Haveman J, van Bree C. Clonogenic assay of cells in vitro. Nature protocols. 2006; 1:2315–2319.
29. Huang, da W.; Sherman, BT.; Lempicki, RA. Systematic and integrative analysis of large gene lists using DAVID bioinformatics resources. Nature protocols. 2009; 4:44–57.
30. Zhang Y, Liu Z, Medrzycki M, Cao K, Fan Y. Reduction of Hox gene expression by histone H1 depletion. PloS one. 2012; 7:e38829. [PubMed: 22701719]
31. Cao K, Lailler N, Zhang Y, Kumar A, Uppal K, Liu Z, et al. High-resolution mapping of h1 linker histone variants in embryonic stem cells. PLoS genetics. 2013; 9:e1003417. [PubMed: 23633960]
32. Yang Y, Hu JF, Ulaner GA, Li T, Yao X, Vu TH, et al. Epigenetic regulation of Igf2/*H19* imprinting at CTCF insulator binding sites. Journal of cellular biochemistry. 2003; 90:1038–1055. [PubMed: 14624463]
33. Hark AT, Schoenherr CJ, Katz DJ, Ingram RS, Levorse JM, Tilghman SM. CTCF mediates methylation-sensitive enhancer-blocking activity at the *H19*/Igf2 locus. Nature. 2000; 405:486–489. [PubMed: 10839547]
34. Bell AC, Felsenfeld G. Methylation of a CTCF-dependent boundary controls imprinted expression of the Igf2 gene. Nature. 2000; 405:482–485. [PubMed: 10839546]
35. Berteaux N, Lottin S, Monte D, Pinte S, Quatannens B, Coll J, et al. *H19* mRNA-like noncoding RNA promotes breast cancer cell proliferation through positive control by E2F1. The Journal of biological chemistry. 2005; 280:29625–29636. [PubMed: 15985428]
36. Lottin S, Adriaenssens E, Dupressoir T, Berteaux N, Montpellier C, Coll J, et al. Overexpression of an ectopic *H19* gene enhances the tumorigenic properties of breast cancer cells. Carcinogenesis. 2002; 23:1885–1895. [PubMed: 12419837]
37. Matouk IJ, DeGroot N, Mezan S, Ayesh S, Abu-lail R, Hochberg A, et al. The *H19* non-coding RNA is essential for human tumor growth. PloS one. 2007; 2:e845. [PubMed: 17786216]

38. Yang F, Bi J, Xue X, Zheng L, Zhi K, Hua J, et al. Up-regulated long non-coding RNA *H19* contributes to proliferation of gastric cancer cells. The FEBS journal. 2012; 279:3159–3165. [PubMed: 22776265]
39. Luo M, Li Z, Wang W, Zeng Y, Liu Z, Qiu J. Long non-coding RNA *H19* increases bladder cancer metastasis by associating with EZH2 and inhibiting E-cadherin expression. Cancer letters. 2013; 333:213–221. [PubMed: 23354591]
40. Barsyte-Lovejoy D, Lau SK, Boutros PC, Khosravi F, Jurisica I, Andrulis IL, et al. The c-Myc oncogene directly induces the *H19* noncoding RNA by allele-specific binding to potentiate tumorigenesis. Cancer research. 2006; 66:5330–5337. [PubMed: 16707459]
41. Li Y, Meng G, Guo QN. Changes in genomic imprinting and gene expression associated with transformation in a model of human osteosarcoma. Experimental and molecular pathology. 2008; 84:234–239. [PubMed: 18501891]
42. Giambra V, Volpi S, Emelyanov AV, Pflugh D, Bothwell AL, Norio P, et al. Pax5 and linker histone H1 coordinate DNA methylation and histone modifications in the 3' regulatory region of the immunoglobulin heavy chain locus. Molecular and cellular biology. 2008; 28:6123–6133. [PubMed: 18644860]
43. Maclean JA, Bettegowda A, Kim BJ, Lou CH, Yang SM, Bhardwaj A, et al. The rhox homeobox gene cluster is imprinted and selectively targeted for regulation by histone h1 and DNA methylation. Molecular and cellular biology. 2011; 31:1275–1287. [PubMed: 21245380]
44. Yang SM, Kim BJ, Norwood Toro L, Skoultchi AI. H1 linker histone promotes epigenetic silencing by regulating both DNA methylation and histone H3 methylation. Proceedings of the National Academy of Sciences of the United States of America. 2013; 110:1708–1713. [PubMed: 23302691]
45. Th'ng JP, Sung R, Ye M, Hendzel MJ. H1 family histones in the nucleus. Control of binding and localization by the C-terminal domain. The Journal of biological chemistry. 2005; 280:27809–27814. [PubMed: 15911621]
46. Orrego M, Ponte I, Roque A, Buschati N, Mora X, Suau P. Differential affinity of mammalian histone H1 somatic subtypes for DNA and chromatin. BMC biology. 2007; 5:22. [PubMed: 17498293]
47. Vaquero A, Scher M, Lee D, Erdjument-Bromage H, Tempst P, Reinberg D. Human SirT1 interacts with histone H1 and promotes formation of facultative heterochromatin. Molecular cell. 2004; 16:93–105. [PubMed: 15469825]
48. Nielsen AL, Oulad-Abdelghani M, Ortiz JA, Remboutsika E, Chambon P, Losson R. Heterochromatin formation in mammalian cells: interaction between histones and HP1 proteins. Molecular cell. 2001; 7:729–739. [PubMed: 11336697]
49. Martin C, Cao R, Zhang Y. Substrate preferences of the EZH2 histone methyltransferase complex. The Journal of biological chemistry. 2006; 281:8365–8370. [PubMed: 16431907]
50. Hill DA, Imbalzano AN. Human SWI/SNF nucleosome remodeling activity is partially inhibited by linker histone H1. Biochemistry. 2000; 39:11649–11656. [PubMed: 10995232]

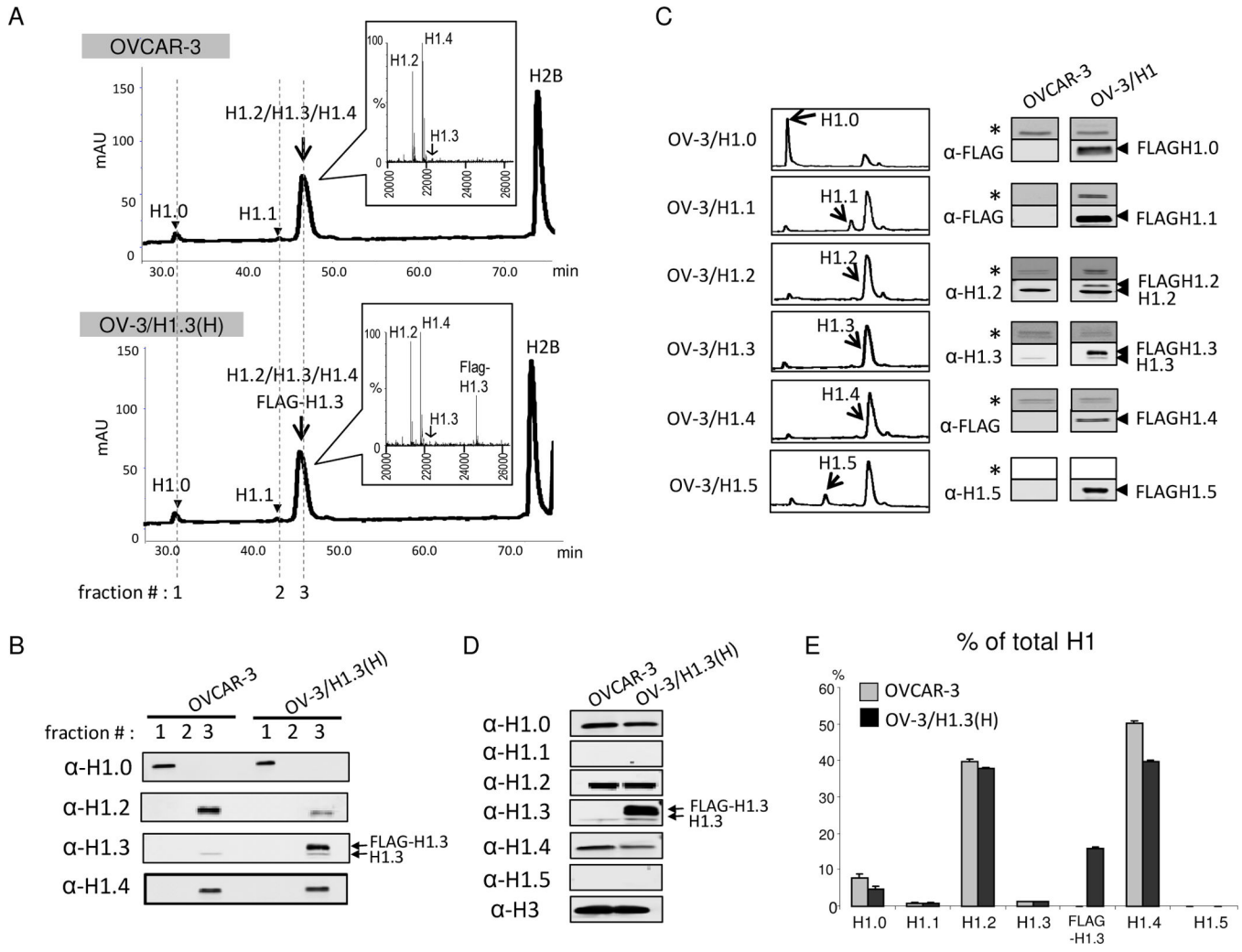

Figure 1. Generation and characterization of OVCAR-3/H1 cells

A) Reverse phase HPLC and mass spectrometry analysis of linker histone H1 variants in OVCAR-3 and OV-3/H1.3(H) cells. Insets: ESI-TOF mass spectrometry profiles of fraction 3 eluted from HPLC.

B) H1 variants in fractions 1, 2, and 3 eluted from HPLC (A) determined by Western blotting. FLAG-H1.3 co-elutes in the same fraction 3 as the endogenous H1.3 protein. H1.1 and H1.5 were not detected by Western blotting.

C) Characterization of peaks eluted from HPLC of histones extracted from OVCAR-3/H1 clones. Histone extracts from stable clones with overexpressed H1 variants were analyzed by HPLC (left). Individual peaks were collected and analyzed by Coomassie and Western blotting using indicated antibodies. Coomassie staining (panels labeled with *) and Western blotting assays for the fractions indicated by arrows are shown (right). Fractions from HPLC peaks not indicated by arrows did not give signals in Western blotting using the respective antibodies. Coomassie staining and Western blotting assays of the corresponding fraction from OVCAR-3 cells are included as controls.

D) The comparison of individual H1 variants in OV-3/H1.3(H) and OVCAR-3 by Western blotting.

E) The percent of total H1. The percentage was determined by the ratio of the A_{214} of respective individual H1 variant to the sum of all H1 peaks. The A_{214} values were adjusted to account for the differences in the number of peptide bonds in each H1 variant.

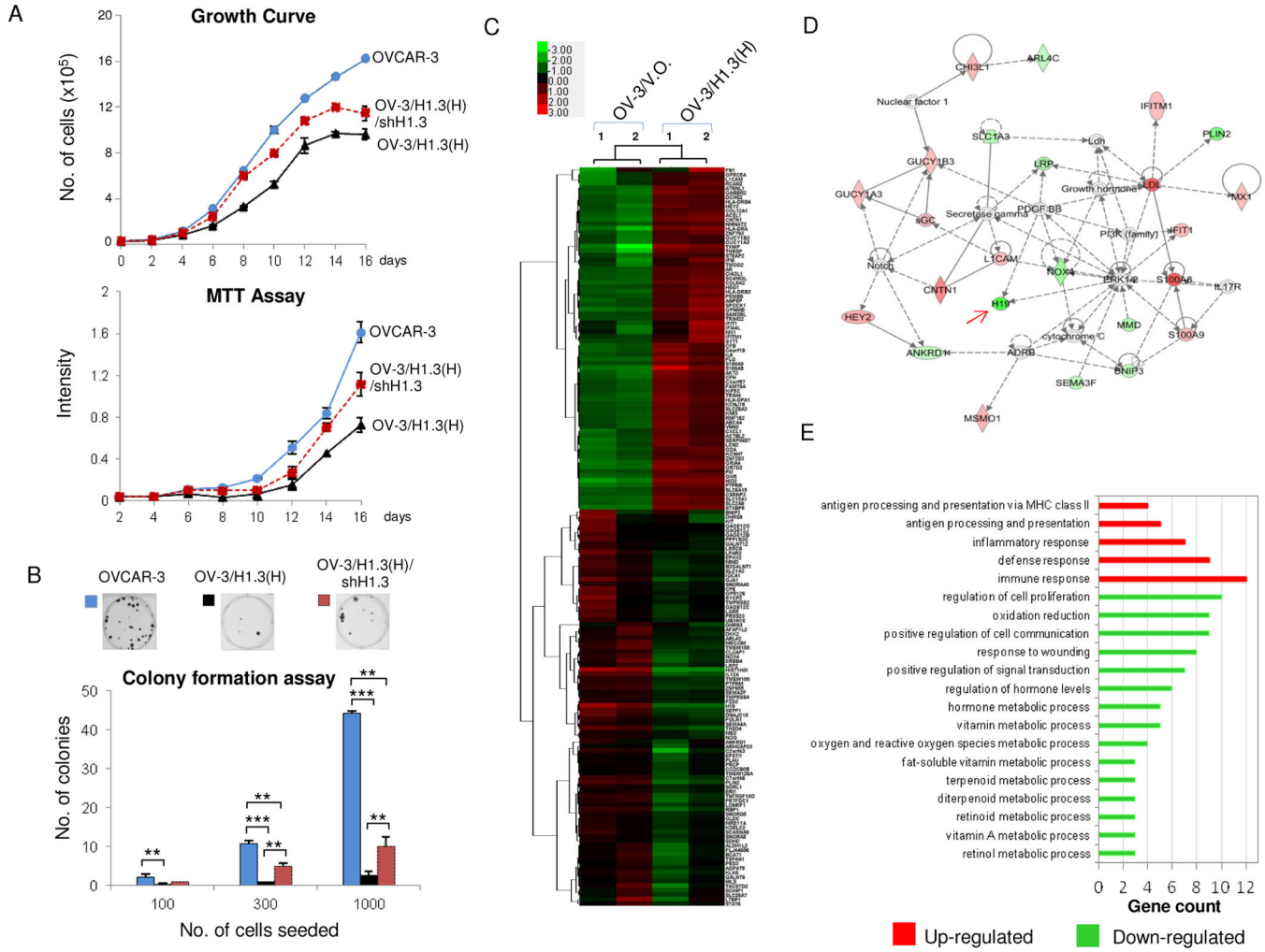

Figure 2. Characterization of OVCAR-3 cells overexpressing H1.3

A) Growth curves and MTT assay of OVCAR-3, OV-3/H1.3(H), and OV-3/H1.3(H)/shH1.3 cells. Data are presented as mean ± SD. P<0.05 for OV-3/H1.3(H) *Vs*. OV-3/H1.3(H)/ shH1.3 as well as other comparisons.

B) Colony formation assay of OVCAR-3, OV-3/H1.3(H), and OV-3/H1.3(H)/shH1.3 cells. Representative results of colony formation assay are shown in insets. The quantitation of colonies formed 4 weeks post seeding (in triplicates). Data are presented as mean ± SD. P values: * < 0.05, **<0.01, ***<0.001.

C) Comparison of global gene changes in OV-3/H1.3(H) and OVCAR-3/V.O. cells. Genes with more than 2-fold expression difference were selected for analysis. The duplicates of OV-3/H1.3(H) and OV-3/V.O. were analyzed and genes were clustered by Cluster 1.0 software.

D) A selected network map with genes altered in OV-3/H1.3(H) clone analyzed by Ingenuity Pathway Analysis. *H19* marked as a gene of interest.

E) Gene Ontology and Functional Annotation Analysis. Genes with increased and decreased expression (≥2-fold) in OV3/H1.3(H) cells were subject to DAVID Gene Ontology analysis and enriched functional categories with P value <0.01 are shown.

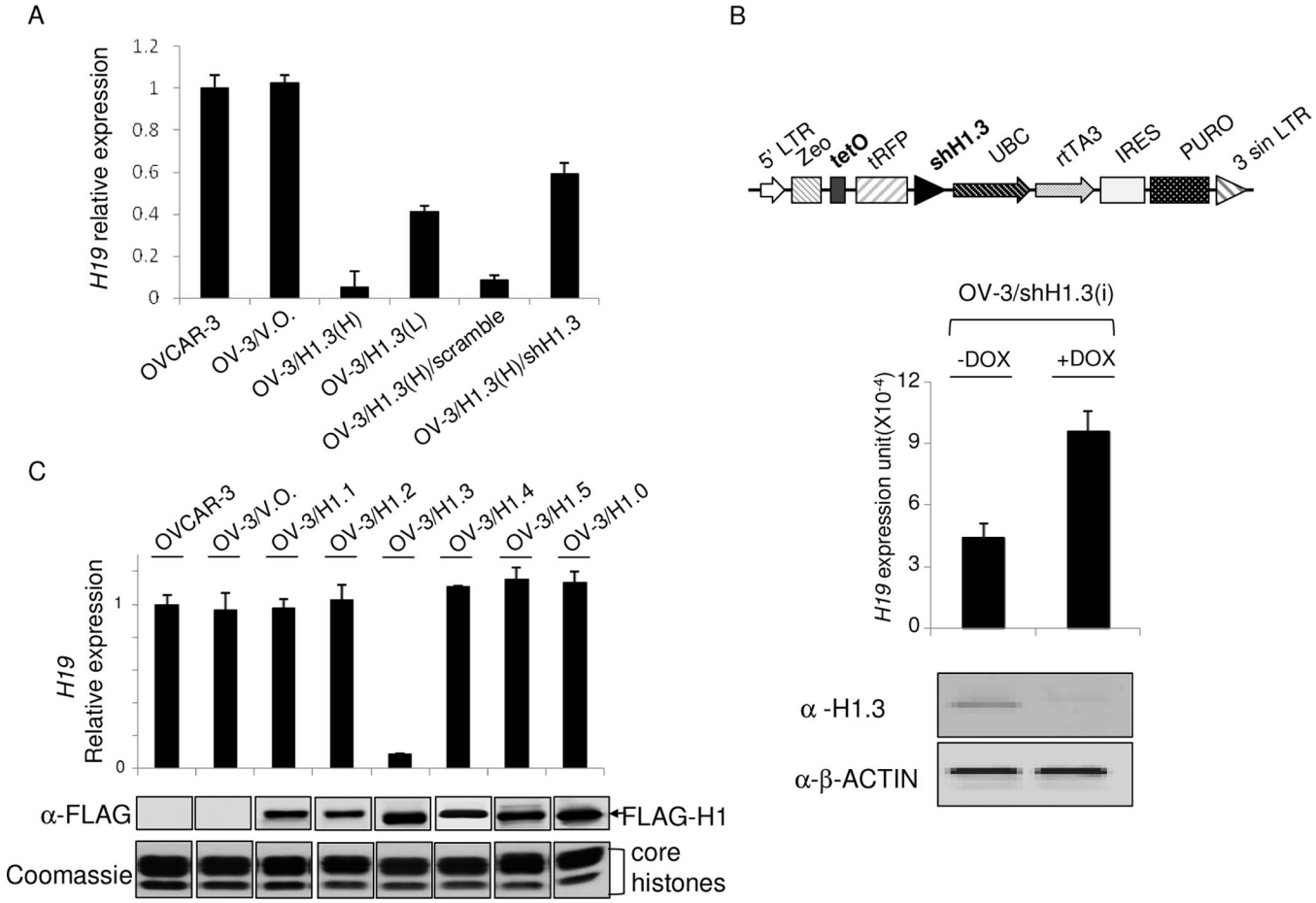

Figure 3. Repression of *H19* expression by H1.3

A) H1.3 overexpression inhibits *H19* expression and knockdown of H1.3 levels in OV-3/H1.3(H) cells mitigates the repression effects on *H19* by H1.3 in OVCAR-3 cells. *H19* expression unit was normalized over *GAPDH*, and *H19* relative expression of each indicated cell line was normalized over OVCAR-3 cells. Bar: SD.

B) Induction of H1.3 knockdown in OV-3/shH1.3(i) cells with Doxycycline increases *H19* expression. Bars: SD. Top: Schematic diagram of pTRIPz-sh*H1.3* inducible vector. Middle: *H19* expression unit measured by RT-PCR and normalized to *GAPDH* expression. Bottom: Western blots of cell lysates using an anti-H1.3 antibody indicating knockdown of H1.3. Western blotting using an anti-β-ACTIN antibody indicates equal loading of cell lysates.

C) Relative expression of the *H19* mRNA transcript level in each indicated cell line measured by qRT-PCR (upper). *H19* expression was measured by qRT-PCR and normalized as described in the legend to A). Bar: SD. 15 μg of total histones were extracted from each cell line and overexpressed exogenous FLAG-H1 levels were analyzed by immunoblotting using an anti-FLAG antibody (middle). Equal loading of histone extracts is indicated by core histones (lower, Commassie stain). OV-3/V.O. cells are OVCAR-3 cells transfected with pcDNA vector without inserted H1 genes.

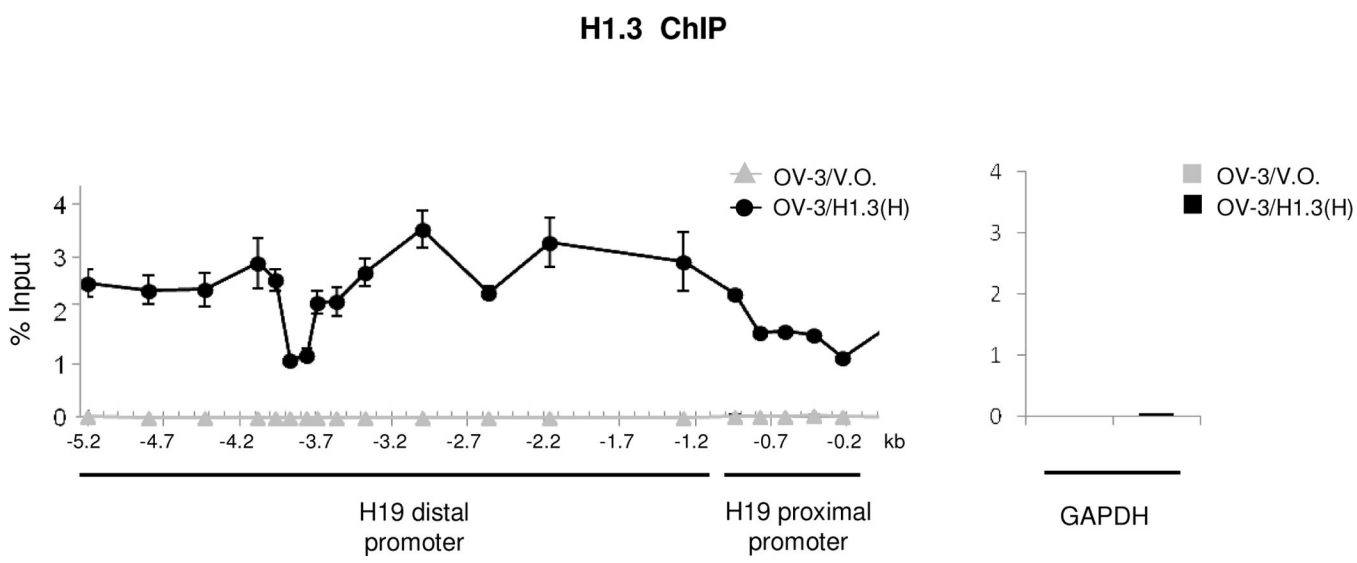

Figure 4. Overexpression of histone H1.3 leads to preferential increases in H1.3 occupancy at *H19*-ICR

qChIP analysis of FLAG-H1.3 along *H19* regulatory regions (left) and *GAPDH* (right) in OV-3/H1.3(H) and OV-3/V.O. cells. Bars: SD.

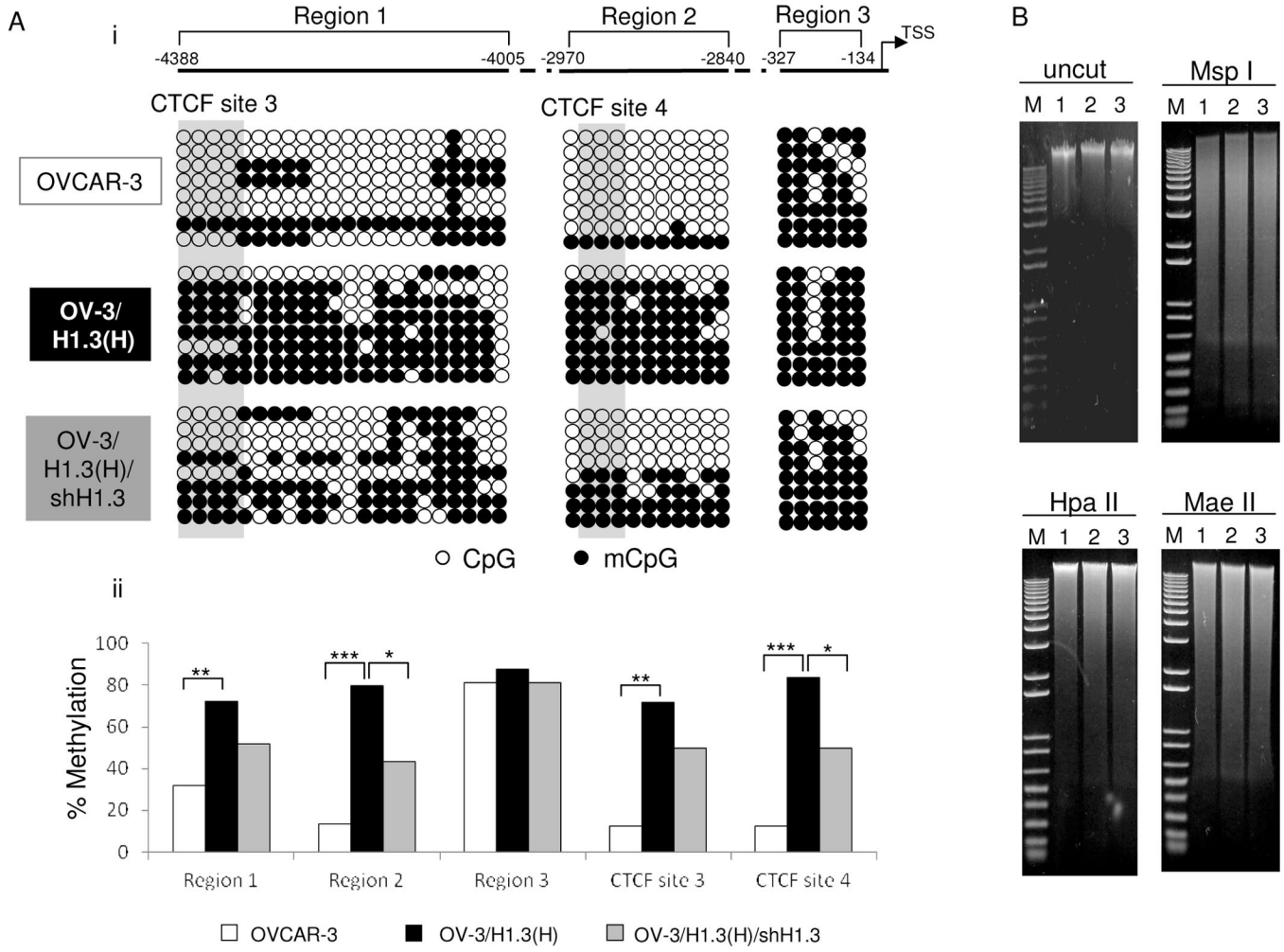

Figure 5. Increased expression of H1.3 leads to DNA methylation elevation at *H19*-ICR in OVCAR-3 cells

A) Bisulfite sequencing analysis of DNA methylation (i) and % of methylated CpG (ii) at CTCF containing regions (Region 1 and 2) and *H19* proximal promoter regions (Region 3) in indicated cell lines. *: $p<0.05$, **: $p<0.01$, ***: $p<0.001$.

B) Global DNA methylation unchanged by H1.3 overexpression. 500 ng of genomic DNA was digested by indicated restriction endonucleases, separated by agarose-gel electrophoresis, and visualized by ethidium-bromide staining. 1: OVCAR-3; 2: OV3/ H1.3(H); and 3:OV3/H1.3(H)/shH1.3. All samples have similar sensitivities to DNA methylation sensitive enzymes HpaII and MaeII, which recognize CCGG and ACGT respectively. Undigested genomic DNA (uncut) and DNA digested by the CCGG recognizing / DNA methylation non-sensitive MspI were included as controls.

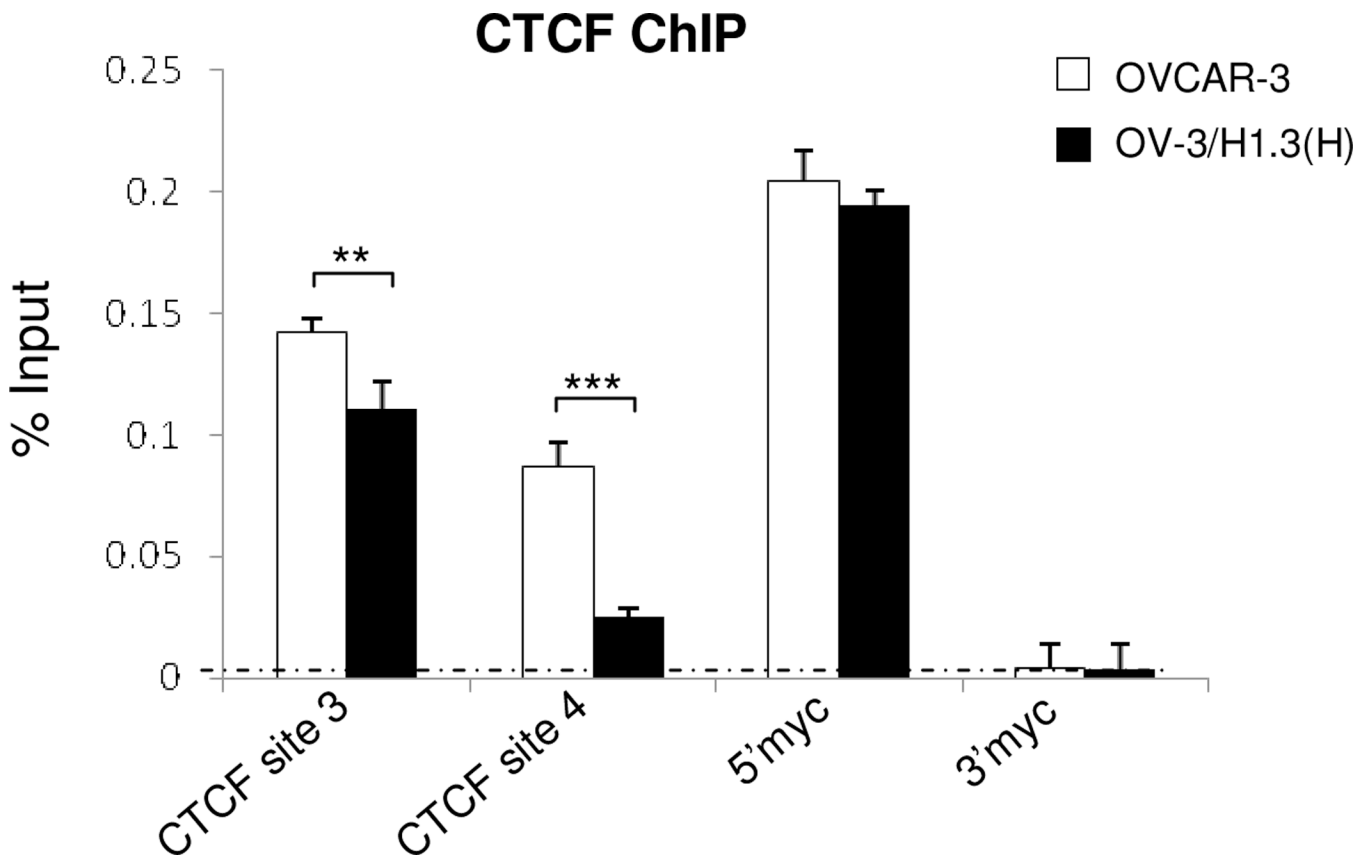

Figure 6. CTCF is partially depleted from *H19*-ICR in OV-3/H1.3(H) cells

qChIP analysis of CTCF in OVCAR-3 and OV3/H1.3(H) cells. The dashed line indicates the highest level of signals detected by qChIP with IgG antibody. The c-myc promoter region (5'myc) containing CTCF binding site and the c-myc downstream region (3'myc) were included as respective positive and negative control sites for CTCF binding. **: $p<0.01$, ***: $p<0.001$.

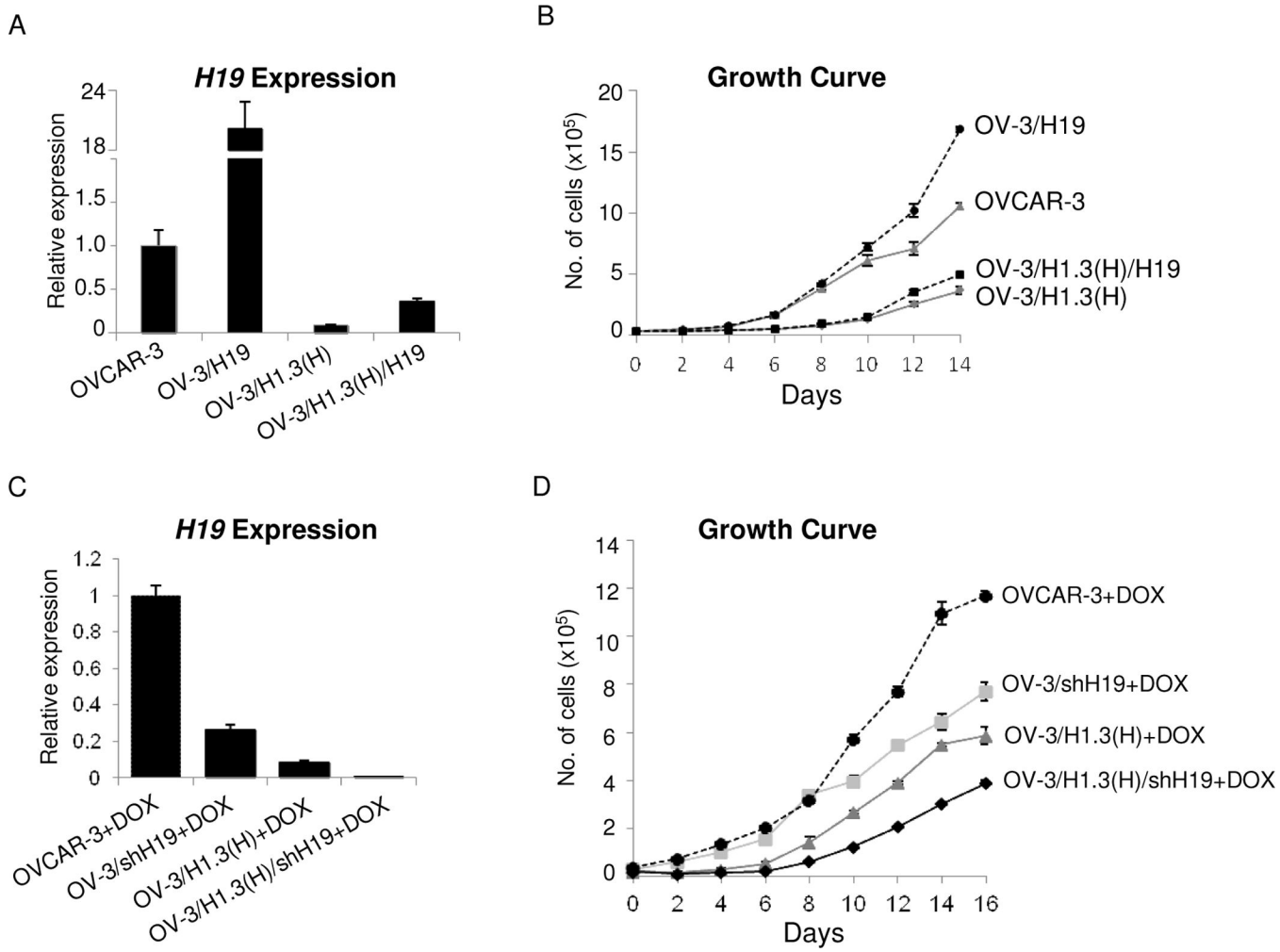

Figure 7. Synergistic effects of H1.3 overexpression and *H19* depletion on OVCAR-3 growth rate

A) RT-PCR analysis of *H19* expression in indicated cell lines. *H19* expression was normalized over *GAPDH*, and *H19* relative expression of each indicated cell line was normalized over OVCAR-3 cells.

B) The growth curves of OV-3/*H19*, OVCAR-3, OV-3/H1.3(H)/*H19*, and OV-3/H1.3(H) cells. Bars: SD; P values < 0.05 for OV-3/H1.3(H)/*H19 Vs*. OV-3/H1.3(H) as well as other comparisons.

C) qRT-PCR analysis of *H19* expression in indicated cell lines. *H19* expression was normalized over *GAPDH*. *H19* expression was measured by qRT-PCR and normalized as described in the legend to A). Bar: SD.

D) The growth curves of OVCAR-3, OV-3/sh*H19*, OV-3/H1.3(H), OV-3/H1.3(H)/sh*H19* cell lines. Medium was supplemented with 1 ug/ml Doxycycline for the entire experiment duration. Bars: SD.